Puncta of neuronal nitric oxide synthase (nNOS) mediate NMDA-receptor signalling in the auditory midbrain

Abbreviated title: Nitric oxide signalling in the auditory midbrain

Bas MJ Olthof, Sarah E Gartside and Adrian Rees*

Institute of Neuroscience, Newcastle University, Newcastle upon Tyne, NE2 4HH, UK

*Adrian Rees
Adrian.rees@ncl.ac.uk

Number of pages 35

Number of figures 6

Abstract words 243

Introduction 650

Discussion 1454

Conflict of Interest
The authors have no conflicts of interests.

Acknowledgements

We thank Nick Lesica for generously making available his software for sound stimulation and electrophysiological recording, Vasilis Glykos and Dominika Lyzwa for writing some of the analysis code, and John Garthwaite for advice on drugs for modulating the nNOS pathway. BMJO was supported in part by a PhD studentship from Newcastle University. We are grateful for financial supported from the BBSRC (BB/P003249/1) to AR and SEG, and a Flexigrant from Action on Hearing Loss to AR.

Abstract

Nitric oxide (NO), is a neurotransmitter synthesised in the brain by neuronal nitric oxide synthase (nNOS). Using immunohistochemistry and confocal imaging in the inferior colliculus (IC, auditory midbrain) of the guinea pig (*Cavia porcellus, male and female*), we show that nNOS occurs in two distinct cellular distributions. We confirm that in the cortices of the IC, a subset of neurons show cytoplasmic labelling for nNOS, while in the central nucleus (ICc) such neurons are not present. However, we demonstrate that all neurons in the ICc do in fact express nNOS in the form of discrete puncta found at the cell membrane. Our multi-labelling studies reveal that nNOS puncta form multi-protein complexes with NMDA receptors, soluble guanylyl cyclase (sGC), and PSD95. These complexes are found apposed to glutamatergic terminals indicative of synaptic function. Interestingly, these glutamatergic terminals express both vesicular glutamate transporters 1 and 2 denoting a specific source of brainstem inputs. With *in vivo* electrophysiological recordings of multiunit activity in the ICc, we found that local application of NMDA enhances sound-driven activity in a concentration-dependent and reversible fashion. This response is abolished by blockade of nNOS or sGC indicating that the NMDA effect is mediated solely via the NO and cGMP signalling pathway. This discovery of a ubiquitous, but highly localised expression, of nNOS throughout the ICc and demonstration of the dramatic influence of the NMDA activated NO pathway on sound-driven neuronal activity, imply a key role for NO signalling in auditory processing.

Significance statement

We show that nNOS, the enzyme that synthesises nitric oxide (NO), occurs as puncta in apparently all neurons in the central nucleus of the inferior colliculus (ICc) in the auditory midbrain. Punctate nNOS appears at glutamatergic synapses in a complex with glutamate NMDA receptors, soluble guanylyl cyclase (the NO receptor), and PSD-95 (a protein that anchors receptors and enzymes at the postsynaptic density). We show that NMDA-receptor modulation of sound-driven activity in the ICc is solely mediated by activation of nNOS and soluble guanylyl cyclase. The presence of nNOS throughout this sensory nucleus, argues for a major role of NO in hearing. Furthermore, this punctate form of nNOS expression may exist and have gone unnoticed in other brain regions.

Introduction

Nitric oxide (NO) is a signalling molecule in diverse life-forms (Feelisch and Martin, 1995; Moroz and Kohn, 2011). In the brain, NO is produced through the action of the calcium/calmodulin-dependent enzyme nNOS, and is involved in intra- and inter-cellular signalling in neurons and glia (Garthwaite, 2008; Garthwaite, 2016). NO can act within the cell in which it is produced, or it may diffuse across the cell membrane to act in presynaptic terminals, or, by volume transmission, at more distant sites (O'Dell et al., 1991; Steinert et al., 2008; Hardingham et al., 2013; Bellefontaine et al., 2014; Garthwaite, 2016).

Several studies have shown a functional interaction between glutamate NMDA-receptor activation, nNOS, and soluble guanylyl cyclase (sGC) -the enzyme catalysing the production of cGMP. Calcium ions (Ca^{2+}) entering through the NMDA receptor (Garthwaite et al., 1988) activate nNOS and the NO produced activates sGC (Arnold et al., 1977) leading to increased levels of cGMP.

The functional coupling of the NMDA receptor, nNOS, and sGC suggests they should be in close proximity at glutamatergic synapses so that small intracellular changes in Ca^{2+} can activate nNOS and allow the NO produced to activate its main downstream receptor sGC (Garthwaite, 2008). Several studies have shown that nNOS binds to a scaffolding protein, postsynaptic density protein (PSD) 95 (Brenman et al., 1996). This protein also anchors the NMDA receptor at the postsynaptic membrane (Valtschanoff and Weinberg, 2001; Burette et al., 2002). Furthermore, an isoform of soluble guanylyl cyclase has been shown to bind to PSD95 in brain homogenates (Russwurm et al., 2001). Thus far, however, the four proteins (PSD95, the NMDA receptor, nNOS and sSG) have not been shown to exist as a single complex in native tissue.

Most studies exploring NO signalling in the brain have been in hippocampus, cerebellum, and cortex (Garthwaite et al., 1988; Shibuki and Okada, 1991; Hardingham and Fox, 2006). However, nNOS occurs in many other brain regions including those associated with sensory processing. Despite the presence of nNOS in sensory systems, with a few exceptions (Cudeiro et al., 1994; Steinert et al.,

2008; Steinert et al., 2011; Lima et al., 2014; Yassin et al., 2014; Kopp-Scheinpflug et al., 2015) relatively little attention has been given to the role of NO in such regions. One sensory structure expressing particularly high levels of nNOS is the inferior colliculus (IC) (Endoh et al., 1994). This principal midbrain centre of the auditory pathway processes virtually all ascending auditory information which it integrates with descending projections from the forebrain and non-auditory inputs (Oliver and Cant, 2018).

The IC consists of three subdivisions. The dorsal and lateral cortices (IC_D and IC_L) (Faye Lund and Osen, 1985; Oliver, 2005), contain neurons that express nNOS densely throughout their somata and dendrites (Herbert et al., 1991; Druga and Syka, 1993; Coote and Rees, 2008). Injection of nNOS inhibitors into IC_D influences sound evoked potentials in the cerebral cortex (Iannone et al., 1996) suggesting that NO signalling in these neurons has a functional role in sound processing. The third subdivision is the tonotopically organised central nucleus (IC_C). Its primary inputs are ascending auditory projections from the brainstem, and its output is the main source of input to the higher auditory system. nNOS filled neurons are absent from the greater part of IC_C and occur only at its border with IC_D, suggesting that NO signalling is not a feature of this nucleus (Coote and Rees, 2008).

In contrast to earlier studies, here we report that apparently all neurons in the IC_C *do* contain nNOS, but that this occurs in a previously undescribed punctate form. We demonstrate that nNOS puncta co-exist with NMDA receptors, sGC, and PSD95 forming multi-protein signalling complexes, and these occur in apposition to glutamatergic terminals indicating their synaptic location. We highlight the functional importance of these synapses by showing that NMDA modulates sound-driven activity in the IC_C *in vivo* and this response is mediated via nNOS and sGC.

Materials and Methods

Animals

Experiments were performed in accordance with the terms and conditions of a license (PPL 60/3934) issued by the UK Home Office under the Animals (Scientific Procedures) Act 1986, and with the approval of the Local Ethical Review committee of Newcastle University. Male and female adult pigmented guinea pigs (*Cavia porcellus*) were bred in-house and kept in spacious housing conditions with food and water available ad libitum. Animals were used for experiments between the ages of 40 and 200 days old.

Immunohistochemistry

Tissue collection and preparation

Animals were deeply anaesthetised with pentobarbital and transcardially perfused either with heparinised 0.1M phosphate buffered saline (PBS) followed by 4% paraformaldehyde (PFA) in PBS, or with 4% PFA only. The brains were post fixed overnight in 4% PFA, cryoprotected in 30% sucrose, and stored at -80° C until they were processed. Coronal sections (40 µm) through the IC were cut on a freezing microtome, and collected into PBS. Sections not immediately required were stored in an antifreeze solution (30% ethylene glycol, 30% sucrose, 1% polyvinyl pyrrolidone (PVP)-40 in PBS) (Watson et al., 1986) at -20 °C.

Immunohistochemistry

Sections were washed in PBS (3 x 10 min), incubated in 5 % $NaBH_4$ (20 min) (for antigen retrieval) and washed again in PBS (3x10 min). Sections were then incubated (overnight at 4 °C) with primary antibodies diluted in a 'block buffer' comprising 0.1 % porcine gelatine (BDH), 1 % bovine serum albumin (Sigma) in 50 mM glycine (Fisher) in PBS (with or without 0.05-0.1 % Triton-X; Sigma). In some cases, sections were pre-incubated in block buffer (1-2 h) before addition of the primary antibodies. The following nNOS antibodies were used: rabbit anti-nNOS (1:2000, Sigma-Aldrich Cat# N7280, RRID:AB_260796); mouse anti-nNOS (1:250-1:500, Sigma-Aldrich Cat# N2280,

RRID:AB_260754); sheep anti-nNOS (1:500, Millipore Cat# AB1529, RRID:AB_90743). We established that all three antibodies resulted in near identical labelling. We also used goat anti-PSD95 (1:1000, Abcam Cat# ab12093, RRID:AB_298846); rabbit anti-sGC α2β1 subunit (1:1000, Abcam Cat# ab42108, RRID:AB_732741); mouse anti-GluN1 (NMDA-R subunit) (1:500, Millipore Cat# MAB363, RRID:AB_94946); goat anti-VGluT1 (1: 500, Synaptic Systems Cat# 135 307, RRID:AB_2619821); rabbit anti-VGluT2 (1:1000, Synaptic Systems Cat# 135 403, RRID:AB_887883); rabbit anti-VGAT (1:1000, Synaptic Systems Cat# 131 003, RRID:AB_887869); rabbit anti-Neurochrom™ (PAN) (which labels somatic, nuclear, dendritic, and axonal neuronal proteins) (1:2000-4000, Millipore Cat# ABN2300, RRID:AB_10953966); rabbit anti-GABA (1:500-1:1000, Sigma-Aldrich Cat# A2052, RRID:AB_477652); mouse anti-NeuN (1:1000, Merck Cat# MAB377, RRID: RRID:AB_2298772). After overnight incubation, sections were washed (3 x 10 min PBS) and incubated for 2 h with secondary antibodies diluted in 5% normal goat serum (Vector Labs) in PBS. The following secondary antibodies were used (all at 1:500 dilution): Alexa Fluor 568 goat anti-rabbit (Thermo Fisher Scientific Cat# A-11036, RRID:AB_10563566); Alexa Fluor 488 goat anti-mouse (Thermo Fisher Scientific Cat# A-11029, RRID:AB_2534088); Alexa Fluor 488 chicken anti-rabbit (Thermo Fisher Scientific Cat# A-21441, RRID:AB_2535859); Alexa Fluor 488 donkey anti-sheep (Thermo Fisher Scientific Cat# A-11015, RRID:AB_2534082); CY5 donkey anti-goat (Abcam Cat# ab97117, RRID:AB_10679586); AMCA donkey anti-mouse (Jackson ImmunoResearch Labs Cat# 715-155-151, RRID:AB_2340807). Sections were washed in PBS (1 x10 min), incubated with the nuclear stain 4', 6-diamidino-2-phenylindole (DAPI, Invitrogen) (10 min, 1-2 nM in PBS), washed in PBS (1 x 10 min) and finally rinsed in distilled water. Sections were mounted on glass slides, air dried, and cover-slipped with Fluoroshield (Sigma). Slides were stored in the dark at 4° C.

For single labelling experiments and double labelling of nNOS and NeuN, nNOS was labelled using rabbit anti-nNOS visualised with Alexa Fluor 488 or 568 goat anti-rabbit secondary. For double labelling of nNOS and PAN, and nNOS and GABA, nNOS and VGAT, as well as triple labelling of nNOS with VGLUT1 and VGLUT2, nNOS was labelled with mouse anti-nNOS visualised with Alex Fluor 488

goat anti-mouse secondary. For the quadruple labelling of nNOS, with PSD95, GluN1 (hereafter called NMDA-R), and sGC, nNOS was labelled with sheep anti-nNOS visualised with Alexa Fluor 488 donkey anti-sheep.

For each antigen and combination, three sections, collected along the rostral caudal axis of the IC, from at least four different animals were labelled. Sections processed and incubated with secondary antibodies in the absence of primary antibody were included as controls.

Image acquisition and analysis

To examine the distribution of labelling throughout the IC, low power (x20) mosaics were acquired using a Zeiss AxioImager with ZenPro software™. Tiles were stitched during image acquisition and images were deconvolved using Huygens Essential (SVI)™. To examine the subcellular distribution of antibody labelling and the proximity of different labels, Z-stacks (Z step 0.1 - 0.3 µm) were acquired using a 60x oil immersion objective on a Nikon A1+ point scanning confocal microscope with Nikon Elements software™. The microscope was equipped with four solid state lasers at 405, 488, 561 and 647 nm. Images were acquired at resolution of 1024 pixels in the XY dimension. Z dimensions were variable. Pixel dimensions were kept at 60 nm for XY with bit depth 12, look up tables (LUTs) were kept linear and covered the full range of the data collected. Z-stacks for all the required antibody combinations were acquired from three sections, collected along the rostral caudal axis of the IC, from at least four different animals. In every section, two Z-stacks were acquired from each region. Z stacks were deconvolved using Huygens Essential (SVI)™ using a theoretical point spread function (PSF), automated background estimation, deconvolved with the Classic Maximum Likelihood Estimation (CMLE) algorithm, quality threshold 0.05 with a maximum number of iterations set at 100. The deconvolved Z-stacks were subsequently analysed using Imaris™ v9.0 (Bitplane.com). To examine the proximity of the nNOS puncta to puncta labelled for PSD-95, sGC and NMDA-R, all labelled puncta were first defined using the 'spot' function. Around each nNOS spot we created a sphere of interest with a radius of 0.2 µm. This value was chosen on the basis of the average length of a postsynaptic density being 0.2-0.8 µm (Sheng and Hoogenraad, 2007). Using the 'Co-localize-

Spot' function, we then identified the population of nNOS spots which were in close proximity to at least one PSD-95 spot (i.e. within the sphere). Next, we determined how many of these nNOS and PSD-95 containing spheres also contained one or more NMDA-R spots. Finally, we determined how many of the nNOS/NMDA-R/PSD-95 containing spheres also contained one or more sGC spots. This allowed us to calculate the proportion of nNOS puncta which were in close proximity to PSD-95 *and* NMDA-R *and* sGC puncta.

To examine the proximity of nNOS puncta to specific subtypes of glutamatergic terminals we first rendered VGluT1 and VGluT2 labelling using the 'spot' function. Next to define populations of terminals labelled for VGluT1 only, VGluT2 only and for both VGluT1 & 2, we used 'co-localise spots' within a sphere of 0.1 µm. Finally, to determine whether individual nNOS puncta were in close proximity to the three populations of glutamatergic terminals we used the 'co-localize spot' function and a sphere of 0.6 µm radius around the nNOS punctum as our definition of close proximity.

In vivo electrophysiological recording

Surgical preparation

Animals were anaesthetised with a combination of urethane (1 $mg.kg^{-1}$ ip, Sigma), fentanyl (0.3 $mg.kg^{-1}$ ip, Hameln) and midazolam (5$mg.kg^{-1}$ im, Hameln). Following induction, animals received supplementary doses of fentanyl as required to prevent a withdrawal response to a hind toe pinch. Atropine (0.05 $mg.kg^{-1}$ sc) was also administered to suppress bronchial secretions. A tracheotomy was performed and the animal was allowed to respire freely in an atmosphere enriched with medical oxygen, or artificially respired as required with oxygen using a modified small animal respirator (Harvard Apparatus). The animal was transferred to a sound attenuated room and fixed in a modified stereotaxic frame (Kopf) equipped with ear bars with Perspex specula positioned to allow an unobstructed view of the tympanic membrane. The animal's body temperature was monitored with a rectal probe and maintained at 38°C with a thermostatically controlled electric heating pad (Harvard Apparatus).

A craniotomy was performed over either the left or right IC, and the cerebral cortex overlying the IC was aspirated. Concentric microdialysis probes (3 mm dialysing window; AN69 Hospal™ membrane) were manufactured in-house by threading 2 sections of silica fused fibre (ID 110 µm /OD 170 µm, SGE Analytical Science) through a Y-shaped body constructed of tubular stainless steel (Goodfellow (AISI 304 (Fe/Cr18/Ni10) diameter 0.5 mm, wall thickness 0.06 mm) glued with Araldite™. A probe was implanted under visual control into the IC, directed medio-laterally at 10° from the vertical, to a depth of approximately 4 mm below the surface of the IC. The microdialysis probe was constantly perfused (2 µl/min) with artificial cerebrospinal fluid (aCSF) (composition (mM) NaCl 140, KCl 3, Na_2HPO_4 0.707, $NaHPO_4$ 0.272, $MgCl_2$ 1, D-glucose 10, and $CaCl_2$ 2.4). Microdialysis provided an effective means of delivering drugs directly into the brain. Because drugs diffuse across the membrane no mechanical perturbation occurs as the drug is applied (Orton and Rees, 2014).

A recording probe with 32-channels arranged linearly over 3.2 mm (100 µm spacing; Neuronexus A1x65-10mm-100-177-A32 50) was implanted vertically in the IC immediately rostral to the microdialysis probe. The depth of the electrode was adjusted to capture responses to the widest range of sound frequencies based on frequency response areas (Palmer et al., 2013) derived from the recorded activity.

Sound stimuli and recording

The electrode was connected to a head stage (NN32AC Tucker Davis Technologies (TDT)) connected to 32 channel preamplifier (PZ2-32, TDT) connected by an optical interface to a BioAmp (RZ2, TDT). Electrophysiological data were sampled at 24.414 kHz. Multi-unit activity was recorded from all 32 channels in response to pure tones (75 ms duration, 10 ms rise/fall time, total sweep duration 150 ms) at 256, 512, 1024, 2048 and 4096 Hz, presented at nominal levels of 50 and 70 dB sound pressure level generated by a Multi-I/O Processor (RZ6, TDT) at a sampling rate of 97.656 kHz. Tones were delivered to the animal with Sony MDR 464 earphones housed in alloy enclosures coupled to damped probe tubes that fitted into the Perspex specula (Rees, 1990). PSTHs were generated from multi-unit activity collected over 150 stimulus repeats for each frequency and level. Matlab scripts

were used to control stimulus presentation, data recording and to store recorded spike data for off-line analysis.

Drug application

Following a baseline period of recording (minimum 1h, beginning at least 1h after implantation of the electrode) during which aCSF was perfused through the dialysis probe, the perfusate was switched to aCSF containing one or more drugs (NMDA (Sigma) (30, 100, 300 µM), N^G-Methyl-L-arginine (L-MeArg) also known as N^G-monomethyl-L-arginine (L-NMMA) (Sigma) (1 mM), 1H-[1,2,4]oxadiazolo[4,3-a]quinoxalin-1-one (ODQ) (Sigma) (500 µM)). To obtain a concentration-response measure for NMDA, increasing concentrations of NMDA were perfused for approximately 40 min, interspersed with intervals of approximately 40 min aCSF (washout). For the L-MeArg and ODQ experiments, NMDA (100 µM) was perfused for 40 min followed by 40 min aCSF (washout), then 20 min of L-MeArg or ODQ, then 40 min of NMDA plus L-MeArg or ODQ, 40 min of aCSF, 40 min of NMDA, and finally 40 min of aCSF. PSTH blocks were generated throughout the periods of drug/aCSF perfusion.

We based our perfusion times on the temporal and spatial analysis of the effects of lidocaine infusion by microdialysis reported by Boehnke and Rasmussen (Boehnke and Rasmusson, 2001). We present data from recordings made 20 min after the onset of drug infusion, the time at which in Boehnke and Rasmussen's (2001) analysis drug tissue concentration achieved a maximal and steady level. Washout data presented are from recordings made 40 min after return to perfusion of aCSF.

Analysis

Off-line electrophysiological recordings from all channels were bandpass filtered with cut-off of 300 Hz and 3000 Hz and thresholded at 2.5 times the standard deviation of the spontaneous activity in the baseline block collected during sweeps in which the stimulus was maximally attenuated by 120 dB. For all subsequent blocks, 'activity' was defined as spikes exceeding this threshold. Data were analysed from electrode sites best representing each of the five frequencies: 256, 512, 1024,

2048, and 4096 Hz. For each frequency and level, PSTHs with a binwidth of 1 ms and a duration of 150 ms were constructed from 150 sweeps of thresholded data. The beginning of the sound-driven response was identified and spikes in a window extending 80 ms from that time were summed to give the driven response. Driven and spontaneous response rates, measured during the different drug/washout conditions, were exported to IBM SPSS Statistics V23™ for statistical analysis.

Experimental Design and Statistical Analysis

Immunohistochemistry data cited are descriptive statistics (mean ± SEM (n) where n= number of Z stacks). Measures were made on two Z stacks per ICc, from each of three sections taken from each of four animals (24 Z stacks in total). Z stacks were obtained at x63 magnification with digital zoom and each one contained between 9 and 15 neuronal somata.

Electrophysiological studies were designed to allow within subjects comparisons. Multichannel probes allowed us to gather data from multiple sites in the ICc of individual animals which corresponded to the best response to each of 5 frequencies. Responses were determined for each frequency under different conditions (increasing concentrations of NMDA and washout, or NMDA with or without L-MeArg or ODQ) in groups of n=3 or n=4 animals. After testing for sphericity (Mauchly) the data were analysed using a two way repeated measures ANOVA with 'frequency' and 'drug condition' as within subject factors. Significant main effects were further analysed using planned post hoc paired-sample t-tests (two tailed) on relevant comparisons. These were corrected for multiple comparisons using the Sidak method.

Results

Two different patterns of nNOS distribution in the IC

To elucidate the functional properties of NO in the IC, we first examined the regional, cellular, and subcellular distribution of its synthetic enzyme, nNOS in the guinea pig (*Cavia porcellus*) IC using fluorescence immunohistochemistry. At low magnification, abundant expression of nNOS is apparent in the ICD and ICL, but little or no expression is visible in the ICC (Fig 1a). Many neurons are visible in the ICD and ICL which have nNOS distributed diffusely throughout the cytoplasm of their somata and dendrites (Fig 1b & c). However, at high magnification, scattered among these cytoplasmically labelled neurons (Fig 1c), we observed bright spots of nNOS labelling (Fig 1c) that we dubbed 'nNOS puncta'. The discovery of nNOS puncta prompted us to look more closely at the ICC - a region devoid of cytoplasmically labelled nNOS neurons. Here, again under high magnification, many nNOS puncta (0.4-0.8 μm in diameter) were visible, clustered around nuclei apparently outlining cell somata (Fig 1d). Double labelling for nNOS and the neuronal marker NeuN showed that these cells were neurons and also revealed, surprisingly, that the somata of apparently all neurons in the ICC contain nNOS puncta (Fig 1ei & eii). Double labelling for nNOS and Neurochrom (a pan-neuronal antibody cocktail labelling somatic, nuclear, dendritic, and axonal proteins) indicated that all nNOS puncta are neuronal and that they occur within other neuronal elements as well as somata (Fig 1f & g).

To determine the neurotransmitter phenotype of neurons containing nNOS puncta, we performed double labelling with antibodies for nNOS and GABA. In the ICD and ICL (Fig 1h) as well as in the ICC (Fig 1i), nNOS expression was observed in both GABA positive (Fig 1h & i, open arrows) and GABA negative neurons. Since virtually all IC neurons are either glutamatergic or GABAergic (Oliver et al., 1994; Merchán et al., 2005), GABA negative neurons are likely to be glutamatergic (Fig 1h & i, filled arrows).

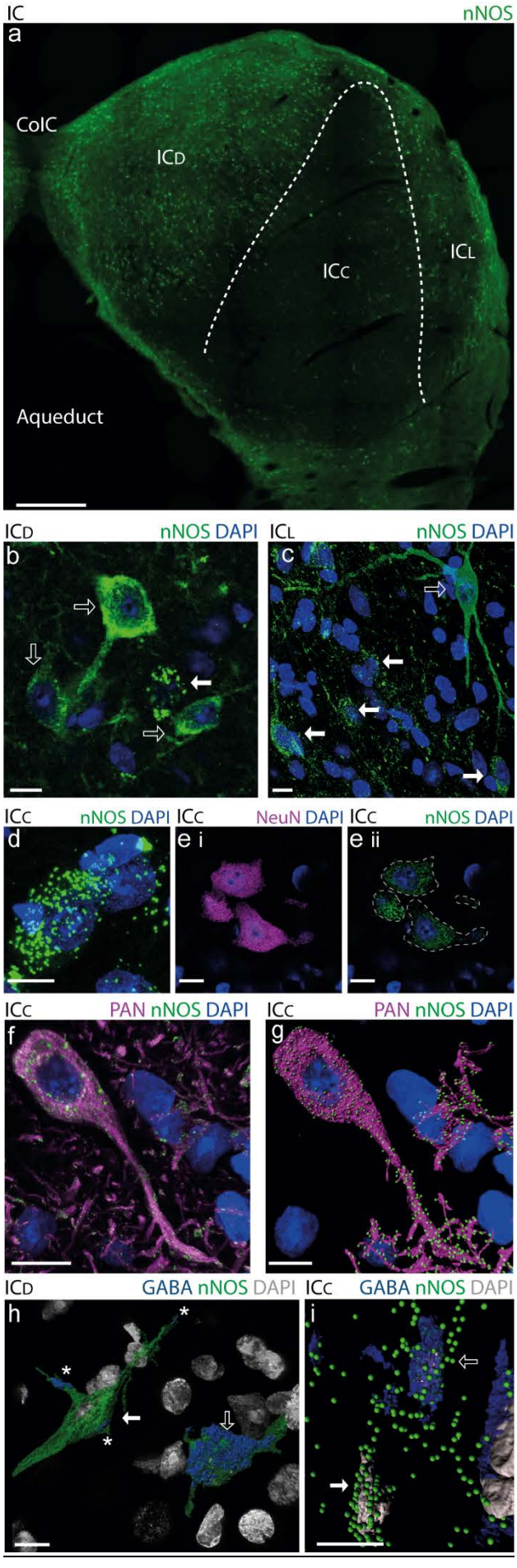

Figure 1

nNOS expression occurs in all subdivisions of the inferior colliculus. ***a)*** *mosaic image of a 40 µm coronal IC section labelled for nNOS (green). nNOS can be seen densely expressed in the dorsal cortex (ICD) and lateral cortex (ICL), while expression is apparently absent from most of the central nucleus (ICC). b) in the ICD there are many neurons with nNOS distributed diffusely throughout their cytoplasm (open arrows). However, puncta of nNOS (closed arrow) surrounding a DAPI stained nucleus (blue) can also be observed in this region.* ***c)*** *in the ICL, large neurons with extensive dendrites completely filled with nNOS are visible (open arrow). Again, however, puncta of nNOS (closed arrow) surrounding a DAPI stained nucleus (blue) can also be observed in this region* ***d)*** *Although the ICC appears devoid of nNOS at low magnification, at higher magnification puncta of nNOS surrounding DAPI stained nuclei are revealed.* ***e)*** *In the ICC, virtually all neurons, visualised by NeuN (ei (magenta)), show signs of punctate nNOS expression (eii (green)): in eii dotted lines outline cell somata visualised by NeuN labelling.* ***f)*** *dual immunohistochemistry for nNOS (green) and a pan neuronal antibody cocktail (PAN, magenta) shows that nNOS labelled puncta are present on the membrane of both somata and dendrites.* ***g)*** *Rendering in Imaris shows clearly how nNOS puncta (green spots) are localised on neuronal elements (magenta surfaces).* ***h)*** *In the ICD, dual immunohistochemistry for nNOS (green) and GABA (blue) rendered in Imaris shows that some nNOS filled cells contain GABA (open arrow), whilst others are GABA negative (closed arrow) and are presumed to be glutamatergic. Note the GABA labelling (asterisks) on the glutamate neuron shown here (closed arrow) is restricted to the surface and therefore considered to be terminals. In contrast, the GABAergic neuron (open arrow) shows GABA labelling throughout its cytoplasm.* ***i)*** *In the ICC, Imaris rendering shows that some cells in the ICC with nNOS puncta (green) also contain GABA (blue, open arrow), while others that do not (closed arrow) and are presumed to be glutamatergic. CoIC: intercollicullar commissure; Aqueduct: aqueduct of Sylvius. Scale bars are 10 µm, except part a) 500 µm.*

Punctate nNOS is structurally associated with PSD95, the NMDA receptor, and sGC.

In the ICc we observed nNOS puncta at the neuronal membrane. We reasoned that, if they occur in close proximity to NMDA receptors and sGC, they could be involved in NMDA receptor neurotransmission. We used high resolution confocal microscopy and image analysis to visualise quadruple immunofluorescence labelling for nNOS, GluN1 (the obligatory subunit of the NMDA receptor), and sGC $\alpha_2\beta_1$ (hereafter sGC), together with PSD95.

Dense, punctate labelling for PSD95 and NMDA-R was found throughout the ICc. Both punctate and diffuse sGC labelling could also be seen within ICc neurons. High resolution confocal imaging revealed considerable overlap between the subcellular distribution of the nNOS puncta (Fig 2ai) and labelling for PSD95 (Fig 2bi), NMDA-R (Fig 2ci), and sGC (Fig 2di). To verify the association between these proteins, their puncta were first rendered to 'spots' using Imaris™ (Fig 2aii-dii). We then, created a sphere of interest, 0.2 μm in diameter, around the centre of each nNOS spot, and determined whether spots for PSD95, NMDA-R and sGC occurred within this sphere (Fig 2e).

Almost all (92 ± 4 %) of the spheres around nNOS puncta contained labelling for PSD95, *and* NMDA-R *and* sGC, demonstrating that nNOS puncta almost always occur in proximity to NMDA, sGC and PSD95 (Fig 2f & g). Interestingly, this analysis revealed a highly consistent order of labelling within the spheres with nNOS and NMDA-R sandwiched between sGC and PSD95 (Fig 2f & g). This consistency suggests that the four protein elements occur in a fixed structural arrangement.

To estimate the extent to which NMDA neurotransmission in the ICc is mediated by NO, we also determined the proportion of the total NMDA-R spots in the ICc that are associated with nNOS. On neuronal somata in the ICc, 84 % (± 5 %) of the NMDA-R spots were associated with nNOS spots. However, at non-somatic sites, presumably dendrites, only 19% (± 6 %) of NMDA-R spots were associated with nNOS spots.

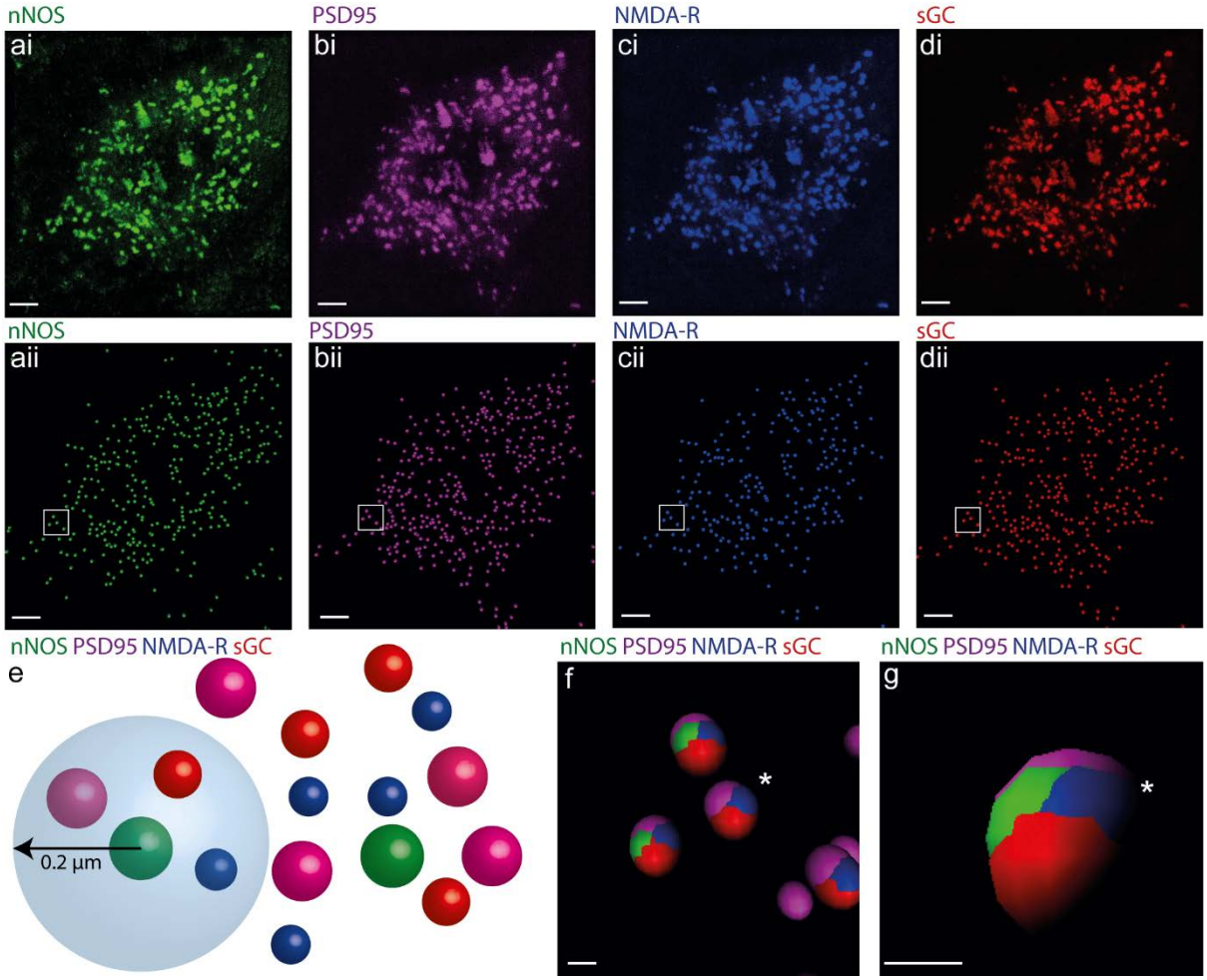

Figure 2

nNOS puncta in the IC are in close proximity to puncta labelled for PSD95, NMDA-R and sGC. ***ai)*** *A cell soma in the ICc showing nNOS puncta (green).* ***bi)*** *the same cell also contains PSD-95 (magenta),* ***ci)*** *the NMDA-R (blue), and* ***di)*** *sGC (red). In* ***aii), bii) cii)*** *and* ***dii)*** *labelled puncta in the raw images ai-di have been rendered to 'spots' in Imaris.* ***e)*** *illustrates how we determined whether individual nNOS puncta were in close proximity to puncta labelled for PSD95, NMDA-R and sGC. A sphere of 0.2 µM radius was centred on each nNOS spot, and the occurrence of PSD95, NMDA-R and sGC spots within this sphere was determined.* ***f)*** *Ellipsoids (shown for the box in aii-dii) are coloured to show the occurrence of the four proteins within the 0.2 µm sphere of interest. Virtually all nNOS spots are in close proximity to spots representing PSD-95, NMDA, and sGC. Note, even where only three colours are seen in this 2D view (cluster marked by *), when the vantage point is changed* ***(g)*** *the fourth colour can be seen. Scale bars in a-d are 10µm, f and g are 1 µm.*

288

nNOS puncta are postsynaptic to glutamatergic terminals

The association of nNOS puncta with NMDA-R suggests they occur at glutamatergic synapses. To test this prediction we determined whether nNOS puncta are associated with labelling for the VGluT1 and VGluT2 subtypes of the presynaptic-terminal vesicular glutamate transporter. To exclude the association of nNOS with GABA and glycine terminals, we also used an antibody against VGAT- the GABA and glycine vesicular transporter.

Confocal imaging and image analysis using Imaris™ revealed three populations of presumed glutamatergic terminals in the ICc: some terminals had labelling for VGluT1 only, others labelled for VGluT2 only, and a third population had labelling for both VGluT1 and VGluT2 within the same terminal. We classified a terminal as 'VGluT1 & 2' when VGluT1 and VGluT2 spots occurred within 0.1 µm of each other.

We saw all three patterns of labelling around neurons containing nNOS puncta in the ICc (Fig 3a). VGluT2 only terminals were particularly abundant, but nNOS spots were rarely close to these terminals (only 3 ± 3 % were within a 0.6 µm diameter sphere). VGluT1 only terminals were less abundant and again nNOS spots were rarely close to them (only 5 ± 2 % were within a 0.6 µm diameter sphere). Although many VGluT1 & 2 terminals were not associated with nNOS puncta, intriguingly, almost all nNOS puncta (89 ± 3 %) coincided with terminals labelling for VGluT1 & 2 (Fig 3cii, dii & eii). Many neurons expressing nNOS puncta also had VGAT labelled terminals around them (Fig 3b). However, proximity testing in Imaris™ never showed any association between puncta labelled for nNOS and VGAT.

These findings provide evidence that nNOS puncta in the ICc are associated with NMDA receptors, sGC and PSD95, and occur at glutamatergic synapses with presynaptic terminals of fibres expressing both VGluT1 & 2.

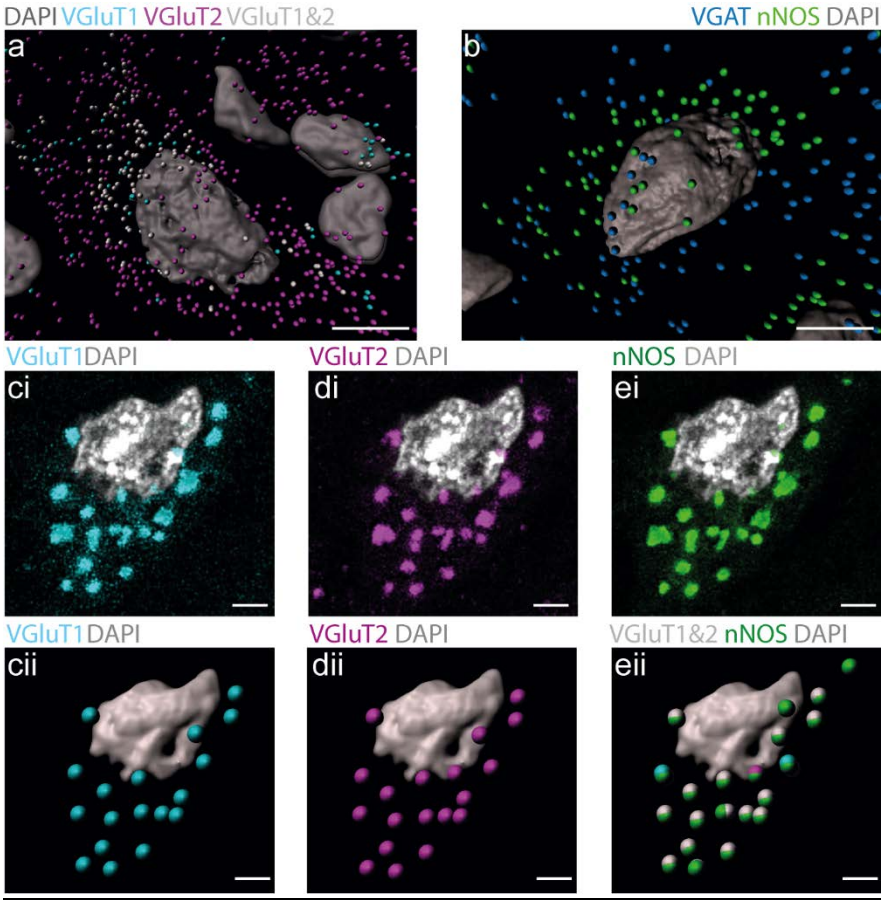

Figure 3

nNOS puncta in the IC are innervated by glutamatergic terminals which predominantly contain both VGluT1 and VGlutT2. ***a)*** *Imaris rendering of a neuron containing nNOS puncta (omitted for clarity) in the ICc showing the distribution of terminals containing VGluT1 only (cyan), VGluT2 only (magenta) and VGluT1 & 2 (white). Note: this neuron receives a substantial number of terminals labelling for VGluT2 only (magenta), a smaller number of terminals labelling for VGluT1 & 2 (white), while terminals labelling for VGluT1 only (cyan) are infrequent.* ***b)*** *Imaris rendering of a cell in the ICc with GABAergic/glycinergic terminals containing VGAT (blue), and nNOS puncta (green). Note: this cell receives GABAergic/glycinergic terminals, but there is no correspondence between these and the nNOS puncta.* ***ci-ei)*** *A slice from a Z-stack showing a neuron from the ICc. Labelling for ci) VGluT1 (cyan); di) VGluT2 (magenta) and ei) nNOS (green).* ***cii-eii)*** *The Z-stacks containing the images in ci-ei were rendered to 'spots' in Imaris representing glutamatergic terminals that contain cii) VGluT1 (cyan) and dii) VGluT2 (magenta). Note almost all the glutamatergic terminals on this cell contain both VGluT1 and VGluT2 as confirmed in eii where terminals labelling for VGluT1 & 2 are shown as white spots. eii also shows that the white spots (VGluT1 & 2 terminals) form ellipsoids with the green spots (nNOS puncta) indicating that they are in close proximity to each other. DAPI stained nuclei are shown in grey. Scale bars in a and b, 10 µm, c-e, 2 µm.*

313

nNOS puncta in the ICc are functional and mediate the effects of NMDA receptor activation

Our immunohistochemical studies demonstrated that punctate nNOS forms a multi-protein complex with NMDA-R and sGC, anchored to PSD95. This suggests that stimulation of these NMDA receptors should lead to the production of NO, which in turn should activate its receptor, sGC to produce cGMP. If this is the case, then inhibition of nNOS or sGC might modulate neuronal responses to NMDA in the ICc. To test this prediction, we conducted electrophysiological recordings in the ICc.

In anaesthetised guinea pigs we used multi-site electrodes to record neuronal activity along the tonotopic axis of the ICc in response to sound. Simultaneously, we delivered drugs targeting NMDA receptors, nNOS, and sGC in the vicinity of the electrodes using microdialysis (Fig 4a, see Methods). Pure tone stimuli (75 ms in duration) were presented at frequencies of 256, 512, 1024, 2048 and 4096 Hz. Peri-stimulus time histograms (PSTHs), constructed from multiunit activity recorded at the five electrode positions maximally activated by these five frequencies, (Fig 4b), typically showed a marked increase in firing with a latency of about 10 ms corresponding to the onset of the tone, followed by a sustained, lower elevation in firing for the remainder of the tone duration.

First we demonstrated that NMDA delivered to the ICc influences sound-driven responses in a concentration dependent manner. After a baseline recording during which artificial cerebrospinal fluid (aCSF) alone was perfused (Fig 4bi), we delivered NMDA in increasing concentrations (30, 100 and 300 µM) (Fig 4bii, iv, & vi) with a washout period of aCSF between each drug application (Fig 4biii, v & vii). As the concentration of NMDA was increased, there was a concomitant increase in the sound-driven activity recorded at all frequency locations (Fig 4c and Table 1). The effect of NMDA was maximal after 20 min, and progressively reversed over the course of 40-50 min during which the NMDA was washed out, although reversal was incomplete after the highest concentration of NMDA (Fig 4bvii & 4c). NMDA also increased spontaneous activity in a concentration-dependent manner (Table 1, see also the 10 ms pre-response period in Fig 4bii, iv & vi). Note, however, that spontaneous activity was 5-10 times below the level of sound-driven activity (Table 1).

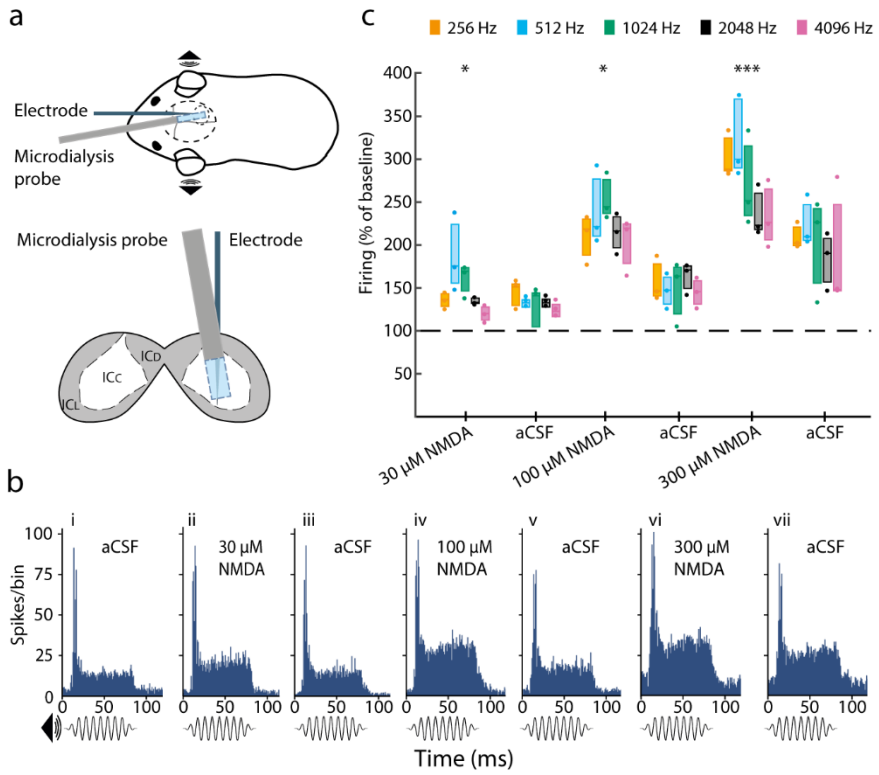

Figure 4

NMDA receptor activation increases sound-driven activity in the ICC in a concentration-dependent and reversible manner. ***a)*** *Above, anaesthetised guinea pigs were implanted with a microdialysis probe and a 32-channel linear recording probe; sound stimuli were delivered to the ears through a closed acoustic system. Below, schematic coronal section through the IC showing the relative positions of the microdialysis probe and the electrode in the ICC.* ***bi-bvii)*** *Example PSTHs of responses to 1024 Hz tone-burst (75 ms duration) during baseline (bi, aCSF) and local perfusion of NMDA at three different concentrations (bii, 30; biv, 100; & bvi, 300 µM) with aCSF washouts (biii, bv, & bvii). Note: the peak of activity at the onset of the sound stimulus and the lower sustained activity during the remainder of the stimulus. NMDA increased the response throughout the stimulus in a concentration dependent manner.* ***c)*** *Group data derived from PSTHs (as in b) revealing local application of NMDA increased sound-driven activity recorded from all of the individual electrode sites with the greatest responses to 256, 512, 1024, 2048 and 4096 Hz. NMDA (30, 100 and 300 µM) increased the response in a concentration-dependent manner at all frequencies, and this effect partially reversed on washout. Data show firing recorded 20 minutes after the start of NMDA perfusion, and for the washout blocks, 40 min after perfusion of aCSF. n = 3 animals. *p<0.05; ***p<0.001 paired sample t-test planned post hoc comparison, Sidak corrected for multiple comparisons, following significant ANOVA. Boxplots show median and interquartile range, together with individual data points.*

Table 1. Effect of increasing concentrations of NMDA on spontaneous and sound-driven activity.

Spontaneous and sound-driven firing rates for each frequency in ICc during perfusion of increasing concentrations of NMDA, or washout with aCSF. The sequence in each column follows the order in Fig 4b. The values are the mean ± SEM of the multiunit firing rate (spikes.s^{-1}) during each stimulus presentation averaged across animals (n=3).

	256 Hz		512 Hz		1024 Hz	
	spontaneous	driven	spontaneous	driven	spontaneous	driven
aCSF	6.6 ± 1.9	46.2 ± 28.1	6.8 ± 0.3	48.4 ± 22.6	7.3 ± 0.9	49.9 ± 39.6
30 µM NMDA	7.5 ± 4.1	62.4 ± 36.3	7.8 ± 3.5	93.7 ± 48.5	10.1 ± 3.0	82.6 ± 69.5
aCSF	8.7 ± 5.7	66.1 ± 43.4	8.1 ± 2.5	65.0 ± 32.6	8.9 ± 1.9	66.7 ± 59.9
100 µM NMDA	14.6 ± 7.0	92.4 ± 49.0	12.3 ± 1.9	118.4 ± 57.5	15.6 ± 2.9	125.2 ± 94.9
aCSF	10.3 ± 4.9	68.2 ± 35.4	6.8 ± 2.2	72.8 ± 41.5	11.1 ± 3.3	81.2 ± 77.7
300 µM NMDA	23.0 ± 12.0	135.4 ± 76.9	16.7 ± 3.3	159.8 ± 76.1	21.8 ± 8.0	131.6 ± 96.3
aCSF	18.5 ± 16.5	94.2 ± 54.7	9.5 ± 2.0	113.0 ± 66.2	13.7 ± 2.2	106.8 ± 97.0

	2048 Hz		4096 Hz	
	spontaneous	driven	spontaneous	driven
aCSF	7.8 ± 3.4	63.6 ± 35.1	6.7 ± 4.1	55.9 ± 20.5
30 µM NMDA	12.1 ± 6.6	86.1 ± 46.9	9.1 ± 6.8	68.9 ± 30.7
aCSF	12.9 ± 6.6	85.0 ± 47.4	13.7 ± 12.8	69.8 ± 26.5
100 µM NMDA	18.8 ± 10.3	142.6 ± 91.9	16.5 ± 10.3	117.5 ± 54.8
aCSF	13.0 ± 8.8	100.5 ± 44.9	10.6 ± 6.7	79.7 ± 22.7
300 µM NMDA	25.5 ± 16.2	157.8 ± 106.8	19.6 ± 10.7	136.9 ± 72.7
aCSF	17.3 ± 10.8	110.7 ± 44.7	13.4 ± 7.6	105.8 ± 46.9

339

Subjecting the data shown in Fig 4c to a two way repeated measures ANOVA revealed a significant main effect of drug condition ($F_{6,12}$=131.2, p<0.0001), but no main effect of frequency ($F_{4,8}$=1.4, n.s.), and no significant condition x frequency interaction ($F_{24,48}$=1.1, n.s.). Activity levels induced by all concentrations of NMDA were significantly different from baseline (average across all frequencies, percent of baseline ± SEM: 30 µM, 148 ± 3.9 %, p=0.018; 100 µM, 225.5 ± 10.1 %, p=0.018; 300 µM, 275.4 ± 2.1 %, p=0.0003. Post hoc t-test with Sidak correction for multiple comparisons).

NMDA-evoked activation of the ICc is mediated by nNOS

To test whether the NMDA-evoked increase in sound-driven activity seen in the previous experiment is mediated by NO, we combined perfusion of NMDA with perfusion of the reversible nNOS inhibitor L-MeArg. Based on the previous experiment, we chose an NMDA concentration of 100 µM for this, since it elicited a robust and readily reversible increase in sound-driven activity.

As before, NMDA (100 µM) evoked an increase in sound-driven activity at all frequencies (Fig 5aii & 5b), and this reversed during washout (Fig 5b). Next we applied L-MeArg (1 mM) immediately followed by L-MeArg (1mM) in combination with NMDA (100 µM). In the presence of L-MeArg alone, sound-driven activity was unaffected at any of the frequencies tested (Fig 5b). Remarkably, when L-MeArg was applied along with NMDA, NMDA failed to elicit any increase in firing (Fig 5aiii & b). To verify that neurons were still capable of responding to NMDA after L-MeArg washed out, we perfused NMDA (100 µM) alone. Again we observed the expected large increase in sound-driven activity (Fig 5aiv).

Two way repeated measures ANOVA confirmed a significant main effect of drug condition ($F_{7,21}$=17.6, p<0.0001), but no significant main effect of frequency ($F_{4,12}$=1.4, n.s.), and no significant condition x frequency interaction ($F_{28,84}$=2.1, n.s.). Post hoc t-tests, Sidak corrected, showed that both the initial and final NMDA-alone conditions, averaged across all frequencies, were significantly different from baseline (217.0 ± 16.3 %, p=0.022 and 231.7 ± 7.01 %, p=0.0013, respectively), while

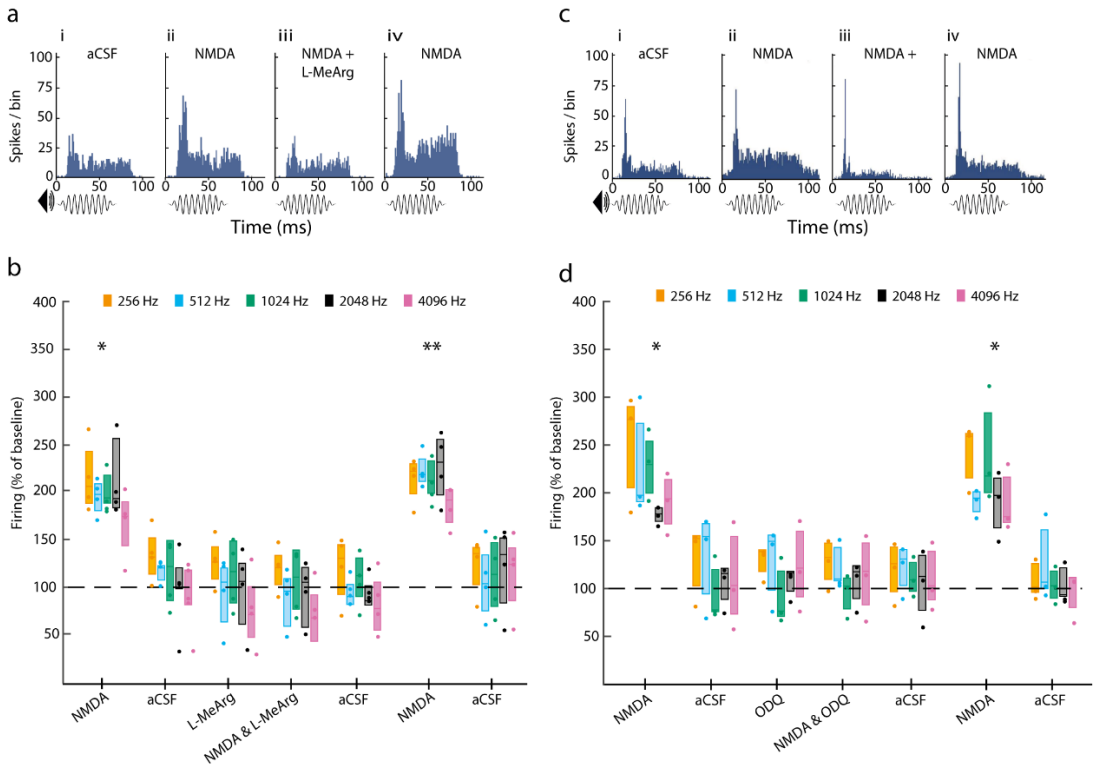

Figure 5

The effect of NMDA is blocked by the inhibition of nNOS and sGC. ***a)*** *Example PSTHs of the response to 1024 Hz tone-bursts during (ai) baseline (aCSF) and perfusion of (aii) NMDA (100 µM) and (aiii) NMDA combined with L-MeArg (1mM). Washout and L-MeArg alone blocks are not shown. Note: (aiii) NMDA fails to increase sound-driven activity in the presence of L-MeArg, but (aiv) its effect is restored after washout of L-MeArg.* ***b)*** *Group data (n=4) derived from PSTHs (as in a) for all frequencies. Perfusion of NMDA (100 µM) increased sound-driven activity at all frequencies. L-MeArg alone had no effect on sound-driven activity, but blocked the response to NMDA. Following washout of L-MeArg, NMDA again increased sound-driven activity.* ***c)*** *Example PSTHs of response to 1024 Hz tone-bursts during (ci) baseline (aCSF) and perfusion of (cii) NMDA (100 µM) and (ciii) NMDA combined with the sGC inhibitor ODQ (500 µM). Washout and ODQ-alone blocks are not shown. Note: (ciii) NMDA fails to increase sound-driven activity in the presence of ODQ, but (civ) its effect is restored after washout of ODQ. d) Group data (n=3) derived from PSTHs (as in c) for all frequencies. Perfusion of NMDA (100 µM) increased the sound-driven activity at all frequencies. ODQ alone had no effect, but blocked the response to NMDA. Following washout of ODQ, NMDA again increased sound-driven activity. Data show firing recorded 20 minutes after the start of drug perfusion, or 40 min after the start of aCSF perfusion. *p<0.05; **p < 0.01 paired sample t-test planned post hoc comparison, Sidak corrected for multiple comparisons, following significant ANOVA. Boxplots show median and interquartile range, together with individual data points.*

364 the L-MeArg alone and L-MeArg plus NMDA conditions were not significantly different from baseline
365 (103.5 ± 19.1 % n.s. and 95.8 ± 17.5 % n.s., respectively).

366 These data are consistent with our hypothesis that modulation of sound-driven activity by the
367 activation of NMDA receptors in the ICc is mediated by the stimulation nNOS leading to the synthesis
368 of NO.

369 *NMDA-evoked activation of the ICc is mediated by sGC*

370 Finally we addressed whether the nNOS dependent response to NMDA observed above also requires
371 the activation of sGC. To examine this, we combined application of NMDA with perfusion of the sGC
372 inhibitor ODQ. Initial perfusion of NMDA (100 μM) evoked an increase in sound-driven activity (Fig
373 5cii & f) which reversed on washout. Next we perfused ODQ (500 μM) alone (Fig 5d) before
374 perfusing NMDA in combination with ODQ (Fig 5d). Sound-driven activity was unaffected with ODQ
375 alone (Fig 5d), and when ODQ was applied along with NMDA, NMDA failed to elicit any increase in
376 firing (Fig 5ciii & f). Finally, following ODQ washout, a further perfusion of NMDA *alone* elicited the
377 expected large increase in sound-driven activity (Fig 5civ & d).

378 A two way repeated measures ANOVA confirmed a significant main effect of drug condition
379 ($F_{7,14}$=21.4, p<0.0001), no significant main effect of frequency ($F_{4,8}$=3.8, n.s.), and no significant
380 condition x frequency interaction ($F_{28,56}$=1.1, n.s.). Post hoc t-tests, Sidak corrected, showed that
381 both the initial and the final NMDA-alone conditions, averaged across all frequencies, were
382 significantly different from baseline (232.5 ± 14.9 % p=0.050 and 231.2 ± 12.4 %, p=0.035
383 respectively), while the ODQ alone and ODQ with NMDA conditions were not significantly different
384 from baseline (113.0 ± 14.9 %, n.s., and 110.8 ± 8.8 %, n.s. respectively).

Discussion

Here we report punctate expression of nNOS in the IC and demonstrate its functional involvement in auditory processing *in vivo*. nNOS expression in the IC is more extensive than previously reported: in addition to cytoplasmically labelled nNOS neurons in the IC cortices, nNOS also occurs in the ICc where it is in the form of puncta. Virtually all these nNOS puncta are associated with NMDA-R, sGC, and PSD95, and apposed to glutamatergic terminals suggesting a postsynaptic multi-protein complex that mediates NMDA-R signalling through the production of NO. The importance of NMDA-receptor and NO signalling in ICc is revealed by *in vivo* experiments that demonstrate the increase in sound-driven neuronal firing by NMDA is completely inhibited by blockade of either nNOS or sGC.

Two distinct patterns of nNOS in the IC

The nNOS expression we report in the cortices of the IC concurs with previous studies showing neurons with diffuse cytoplasmic labelling, are abundant in these subdivisions (Herbert et al., 1991; Druga and Syka, 1993; Coote and Rees, 2008; Hinova-Palova et al., 2017). However, we find nNOS puncta in neurons located in all three subdivisions of the IC. Importantly, vast numbers of nNOS puncta are found in the ICc, indeed virtually all neurons in the ICc, both glutamatergic and GABAergic, contain nNOS puncta. The ubiquitous presence of nNOS in neurons in the ICc may previously have gone unnoticed because it occurs in the form of puncta not visible at low magnification. Interestingly, a recent paper addressing developmental changes in mouse brain included a low power image in which punctate nNOS labelling in the ICc is apparent (Fujimoto et al., 2017), although this was not noted or discussed.

nNOS puncta are structurally associated with PSD95 and with NMDA-R and sGC

In several brain regions, the NMDA receptor has been linked to NO signalling. Given that Ca^{2+} ion entry via NMDA receptors is highly localised, and that NO is only synthesised in pico molar concentrations, it has been postulated that the proteins in this pathway must be in close proximity (Garthwaite, 2008). Previous studies (Kornau et al., 1995; Brenman et al., 1996; Niethammer et al.,

1996; Russwurm et al., 2001) show that nNOS, NMDA-R and sGC can all potentially interact with PSD95. Until now, however, the formation of a multi-protein complex involving all four proteins had not been demonstrated in native tissue. Using quadruple immunohistochemistry, we revealed that virtually all nNOS puncta in the ICc occur close to PSD95, NMDA-R and sGC, confirming that nNOS in the IC exists as part of this multi-protein complex. To the best of our knowledge, this is the first time *all four* proteins have been demonstrated to occur simultaneously at the same postsynaptic site, as illustrated schematically in Fig 6.

In contrast, neurons with cytoplasmic labelling for nNOS in the cortices of the IC, are not associated with the proteins that constitute the multi-protein complex at nNOS puncta. This suggests a less temporally- and spatially-specific mode of action of NO in these neurons, perhaps by volume transmission, as has been shown to occur elsewhere in the auditory pathway (Steinert et al., 2008).

nNOS puncta are innervated by glutamatergic terminals

We found that nNOS puncta at the cell membrane of neurons occur in close apposition to glutamatergic terminals, indicating that they are situated in synapses and likely to be functionally active. A previous report showed punctate nNOS in the hippocampus located on dendritic spines receiving glutamatergic inputs (Burette et al., 2002), as well as occasionally bound to the post synaptic densities of GABAergic synapses (Szabadits et al., 2007). In the IC, we found nNOS puncta are almost exclusively associated with glutamatergic presynaptic terminals identified by the presence of vesicular glutamate transporter proteins (Fremeau et al., 2001; Kaneko and Fujiyama, 2002), and never with GABAergic or glycinergic terminals.

The expression of VGluT1 and VGluT2 in the terminals of fibres in the ICc helps reveal their origin (Ito and Oliver, 2010; Ito et al., 2011). Thus, terminals containing exclusively VGluT1 originate predominantly from **the** cerebral cortex, whereas terminals containing only VGluT2, represent intra-collicular connections, along with ascending inputs from the dorsal cochlear nucleus, some nuclei in the superior olive and the lateral lemniscus (Ito and Oliver, 2010). Terminals containing *both* VGluT1

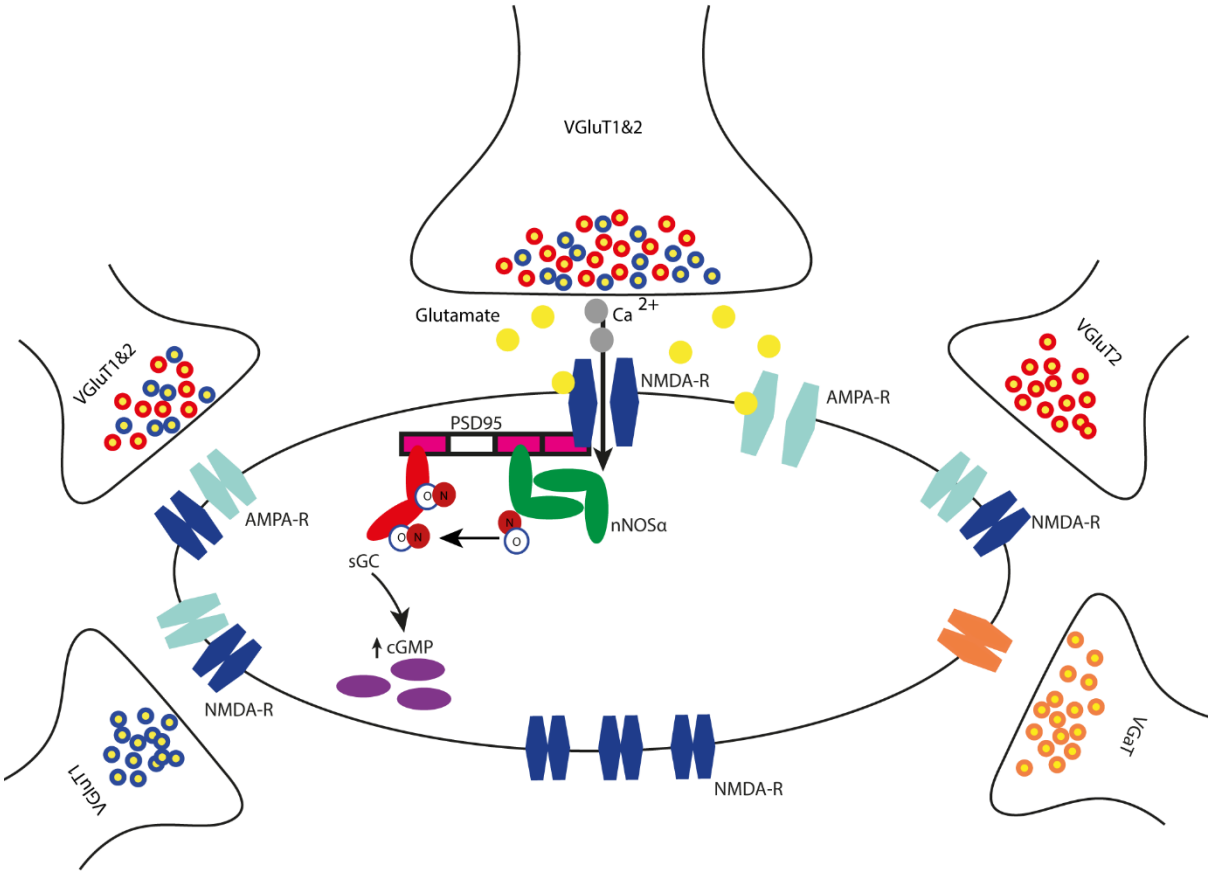

Figure 6

Schematic representation of NO signalling mediating NMDA receptor activation in the central nucleus of the IC. A presynaptic glutamatergic terminal containing both VGluT1 & 2 is in close apposition to a postsynaptic multi-protein complex consisting of NMDA-R, nNOS and sGC, attached to the scaffold protein PSD95. Initial depolarisation by glutamate binding to AMPA receptor, allows the activation of the NMDA receptor. Calcium ions enter the cell through the NMDA receptor and activate nNOS (via calmodulin not shown) leading to the synthesis of NO. NO in turn activates sGC which produces the second messenger cGMP. Other excitatory and inhibitory terminals not terminating on NOSergic multi-protein complexes are shown. Note also the presence of a separate pool of NMDA receptors not linked to the NO signalling pathway.

435

& VGluT2 belong to fibres originating from three principal sources in the brainstem: the contralateral ventral cochlear nucleus (VCN), the ipsilateral medial superior olivary nucleus (MSO), and certain subdivisions of the periolivary nuclei (Ito and Oliver, 2010).

We cannot specify the sources giving rise to the VGluT1 & 2 terminals associated with the nNOS puncta, and there are indeed many VGluT1 & 2 terminals that are not associated with nNOS puncta. However, it seems unlikely that precisely timed inputs from the MSO, (which signal interaural time differences (Grothe et al., 2010)), would terminate at synapses with 'slowly' responding NMDA receptors. More likely these terminals originate from the Type 1 multipolar (or T stellate) neurons in the VCN (Cant and Benson, 2003; Cant and Benson, 2006) which signal information about the spectrum of sounds (Young et al., 1988; Blackburn and Sachs, 1989, 1990; Oertel et al., 2011). If Type 1 multipolar neurons signal through NMDA receptors in the ICc, they could mediate some form of neuronal plasticity.

Potential physiological role of nNOS/sGC signalling in the ICc

Our electrophysiological data show the important influence NO signalling can have in the ICc. Local perfusion of NMDA in the ICc resulted in a substantial and concentration-dependent increase in sound-driven activity. Remarkably, this NMDA-evoked increase in activity was completely blocked when we inhibited nNOS or sGC. These effects are likely to originate in the ICc since substances infused by microdialysis are spatially limited to ~1.5 mm from the probe Boehnke and Rasmussen (Boehnke and Rasmusson, 2001). Furthermore, since neurons in the IC cortices do not project back to the ICc, indirect effects from those subdivisions are unlikely.

Sound stimuli drive neuronal activity in the ICc via multiple parallel excitatory and inhibitory inputs (Oliver, 2005). Glutamatergic inputs have been shown to be mediated by both AMPA and NMDA receptors (Faingold et al., 1989; Zhang and Kelly, 2001) and it is perhaps surprising, that blocking nNOS and sGC had no effect on endogenous glutamatergic signalling in response to sound. Prosaic reasons, relating to the time course and concentration of drug application or sensitivity of our

measure, could explain this finding, but it is interesting that with a different method in a different structure, Yassin et al (2014) similarly found no effect of ODQ when it was applied alone.

It should be noted that while most NMDA receptors on the somata are linked to nNOS, we found many NMDA receptors, particularly on the dendrites, which were not linked to nNOS. The influence of the latter population on sound-driven activity should not be blocked by L-MeArg or ODQ. Thus these two populations of NMDA receptors may be activated under different conditions and serve different functions.

A role for NMDA receptors and nNOS in adaptive and maladaptive changes?

The modulation of neuronal signalling in the ICc through the activation of NMDA receptors and nNOS , suggests the these mechanisms may mediate adaptive or plastic changes in response to sound (Slee and David, 2015). The auditory system is highly plastic and evidence suggests that the IC is particularly so (Yan and Suga, 1998; Suga and Ma, 2003). Sustained NMDA receptor activation subsequent to stimulus or neuromodulatory input will activate nNOS and lead to production of cGMP. Via protein Kinase G, cGMP induces phosphorylation of AMPA receptor subunits and thereby influences the insertion of AMPA receptors into the cell membrane (Serulle et al., 2007; Incontro et al., 2013; Song et al., 2016). This mechanism would enhance neuronal excitability and might underlie the increase in sound-driven activity we observed following NMDA perfusion. In some circumstances, changes in nNOS expression may be maladaptative. Thus increases in neuronal excitability and firing occur in the IC following acoustic trauma (Mulders and Robertson, 2009) or salicylate (Patel and Zhang, 2014; Olthof-Bakker et al., 2017). These changes could depend on the upregulation of nNOS, as has been demonstrated in the cochlear nucleus in similar animal models of tinnitus (Zheng et al., 2006; Coomber et al., 2015).

Wider implications

The discovery of extensive punctate nNOS expression in the ICc has important implications for our understanding of neuronal mechanisms of sound processing in the IC and the auditory pathway. But

these findings also have implications beyond the auditory system. The discovery of nNOS puncta in a region previously thought to be devoid of nNOS highlights the fact that nNOS expression, and by extension NO signalling, may have gone unnoticed in other brain regions. Our finding of two distinct subcellular distributions may lead to a new understanding of how NO contributes to neuronal processing.

Author contributions

BMJO, SEG and AR designed the research; BO performed the experiments with assistance from SEG and AR; BMJO analysed the data with assistance from SEG and AR; BMJO, SEG and AR wrote the paper.

References

Arnold WP, Mittal CK, Katsuki S, Murad F (1977) Nitric oxide activates guanylate cyclase and increases guanosine 3':5'-cyclic monophosphate levels in various tissue preparations. Proceedings of the National Academy of Sciences 74:3203-3207.

Bellefontaine N, Chachlaki K, Parkash J, Vanacker C, Colledge W, d'Anglemont de Tassigny X, Garthwaite J, Bouret SG, Prevot V (2014) Leptin-dependent neuronal no signaling in the preoptic hypothalamus facilitates reproduction. The Journal of Clinical Investigation 124:2550-2559.

Blackburn CC, Sachs MB (1989) Classification of unit types in the anteroventral cochlear nucleus - pst histograms and regularity analysis. J Neurophysiol 62:1303-1329.

Blackburn CC, Sachs MB (1990) The representations of the steady-state vowel sound /e/ in the discharge patterns of cat anteroventral cochlear nucleus neurons. J Neurophysiol 63:1191-1212.

Boehnke SE, Rasmusson DD (2001) Time course and effective spread of lidocaine and tetrodotoxin delivered via microdialysis: An electrophysiological study in cerebral cortex. J Neurosci Methods 105:133-141.

Brenman JE, Chao DS, Gee SH, McGee AW, Craven SE, Santillano DR, Wu Z, Huang F, Xia H, Peters MF, Froehner SC, Bredt DS (1996) Interaction of nitric oxide synthase with the postsynaptic density protein PSD-95 and α1-syntrophin mediated by PDZ domains. Cell 84:757-767.

Burette A, Zabel U, Weinberg RJ, Schmidt HHHW, Valtschanoff JG (2002) Synaptic localization of nitric oxide synthase and soluble guanylyl cyclase in the hippocampus. J Neurosci 22:8961-8970.

Cant NB, Benson CG (2003) Parallel auditory pathways: Projection patterns of the different neuronal populations in the dorsal and ventral cochlear nuclei. Brain Res Bull 60:457-474.

Cant NB, Benson CG (2006) Organization of the inferior colliculus of the gerbil (*meriones unguiculatus*): Differences in distribution of projections from the cochlear nuclei and the superior olivary complex. J Comp Neurol 495:511-528.

Coomber B, Kowalkowski VL, Berger JI, Palmer AR, Wallace MN (2015) Modulating central gain in tinnitus: Changes in nitric oxide synthase in the ventral cochlear nucleus. Frontiers in Neurology 6.

Coote EJ, Rees A (2008) The distribution of nitric oxide synthase in the inferior colliculus of guinea pig. Neuroscience 154:218-225.

Cudeiro J, Rivadulla C, Rodriguez R, Martinezconde S, Acuna C, Alonso JM (1994) Modulatory influence of putative inhibitors of nitric-oxide synthesis on visual processing in the cat lateral geniculate- nucleus. J Neurophysiol 71:146-149.

529 Druga R, Syka J (1993) NADPH-diaphorase activity in the central auditory structures of the rat.
530 Neuroreport 4:999-1002.
531 Endoh M, Maiese K, Wagner JA (1994) Expression of the neural form of nitric oxide synthase by ca1
532 hippocampal neurons and other central nervous system neurons. Neuroscience 63:679-689.
533 Faingold CL, Hoffmann WE, Caspary DM (1989) Effects of excitant amino acids on acoustic responses
534 of inferior colliculus neurons. Hear Res 40:127-136.
535 Faye Lund H, Osen KK (1985) Anatomy of the inferior colliculus in rat. Anat Embryol (Berl) 171:1-20.
536 Feelisch M, Martin JF (1995) The early role of nitric oxide in evolution. Trends in Ecology & Evolution
537 10:496-499.
538 Fremeau RT, Jr., Troyer MD, Pahner I, Nygaard GO, Tran CH, Reimer RJ, Bellocchio EE, Fortin D,
539 Storm-Mathisen J, Edwards RH (2001) The expression of vesicular glutamate transporters
540 defines two classes of excitatory synapse. Neuron 31:247-260.
541 Fujimoto H, Konno K, Watanabe M, Jinno S (2017) Late postnatal shifts of parvalbumin and nitric
542 oxide synthase expression within the gabaergic and glutamatergic phenotypes of inferior
543 colliculus neurons. J Comp Neurol 525:868-884.
544 Garthwaite J (2008) Concepts of neural nitric oxide-mediated transmission. Eur J Neurosci 27:2783-
545 2802.
546 Garthwaite J (2016) From synaptically localized to volume transmission by nitric oxide. J Physiol
547 594:9-18.
548 Garthwaite J, Charles SL, Chess-Williams R (1988) Endothelium-derived relaxing factor release on
549 activation of NMDA receptors suggests role as intercellular messenger in the brain. Nature
550 336:385-388.
551 Grothe B, Pecka M, McAlpine D (2010) Mechanisms of sound localization in mammals. Physiol Rev
552 90:983-1012.
553 Hardingham N, Fox K (2006) The role of nitric oxide and GluR1 in presynaptic and postsynaptic
554 components of neocortical potentiation. J Neurosci 26:7395-7404.
555 Hardingham N, Dachtler J, Fox K (2013) The role of nitric oxide in pre-synaptic plasticity and
556 homeostasis. Front Cell Neurosci 7:190.
557 Herbert H, Aschoff A, Ostwald J (1991) Topography of projections from the auditory cortex to the
558 inferior colliculus in the rat. J Comp Neurol 304:103-122.
559 Hinova-Palova D, Landzhov B, Dzhambazova E, Edelstein L, Minkov M, Fakih K, Minkov R, Paloff A,
560 Ovtscharoff W (2017) NADPH-diaphorase-positive neurons in the human inferior colliculus:
561 Morphology, distribution and clinical implications. Brain Structure and Function 222:1829-
562 1846.

563 Iannone M, DelDuca C, Granato T, Rispoli V, Nistico G (1996) Sound-evoked electrocortical
564 desynchronization is inhibited by n omega-nitro-l-arginine methyl ester microinfused into
565 the inferior colliculi in rats. Electroencephalogr Clin Neurophysiol 99:57-62.
566 Incontro S, Ciruela F, Ziff E, Hofmann F, Sánchez-Prieto J, Torres M (2013) The type II cGMP
567 dependent protein kinase regulates GluA1 levels at the plasma membrane of developing
568 cerebellar granule cells. Biochimica et Biophysica Acta (BBA) - Molecular Cell Research
569 1833:1820-1831.
570 Ito T, Oliver DL (2010) Origins of glutamatergic terminals in the inferior colliculus identified by
571 retrograde transport and expression of vglut1 and vglut2 genes. Front Neuroanat 4:135.
572 Ito T, Bishop DC, Oliver DL (2011) Expression of glutamate and inhibitory amino acid vesicular
573 transporters in the rodent auditory brainstem. J Comp Neurol 519:316-340.
574 Kaneko T, Fujiyama F (2002) Complementary distribution of vesicular glutamate transporters in the
575 central nervous system. Neurosci Res 42:243-250.
576 Kopp-Scheinpflug C, Pigott BM, Forsythe ID (2015) Nitric oxide selectively suppresses ih currents
577 mediated by hcn1-containing channels. J Physiol 593:1685-1700.
578 Kornau HC, Schenker LT, Kennedy MB, Seeburg PH (1995) Domain interaction between NMDA
579 receptor subunits and the postsynaptic density protein PSD-95. Science 269:1737-1740.
580 Lima MG, Maximino C, Matos Oliveira KR, Brasil A, Crespo-Lopez ME, Batista EdJO, Rocha FAdF,
581 Picanço-Diniz DLW, Herculano AM (2014) Nitric oxide as a regulatory molecule in the
582 processing of the visual stimulus. Nitric Oxide 36:44-50.
583 Merchán M, Aguilar LA, Lopez-Poveda EA, Malmierca MS (2005) The inferior colliculus of the rat:
584 Quantitative immunocytochemical study of GABA and glycine. Neuroscience 136:907-925.
585 Moroz LL, Kohn AB (2011) Parallel evolution of nitric oxide signaling: Diversity of synthesis and
586 memory pathways. Front Biosci (Landmark Ed) 16:2008-2051.
587 Mulders WHAM, Robertson D (2009) Hyperactivity in the auditory midbrain after acoustic trauma:
588 Dependence on cochlear activity. Neuroscience 164:733-746.
589 Niethammer M, Kim E, Sheng M (1996) Interaction between the c terminus of NMDA receptor
590 subunits and multiple members of the PSD-95 family of membrane-associated guanylate
591 kinases. J Neurosci 16:2157-2163.
592 O'Dell TJ, Hawkins RD, Kandel ER, Arancio O (1991) Tests of the roles of two diffusible substances in
593 long-term potentiation: Evidence for nitric oxide as a possible early retrograde messenger.
594 Proceedings of the National Academy of Sciences 88:11285-11289.
595 Oertel D, Wright S, Cao XJ, Ferragamo M, Bal R (2011) The multiple functions of t
596 stellate/multipolar/chopper cells in the ventral cochlear nucleus. Hear Res 276:61-69.

Oliver DL (2005) Neuronal organisation of the inferior colliculus. In: The inferior colliculus (Winer JA, Schreiner CE, eds), pp 69-114. New York: Springer.

Oliver DL, Cant NB (2018) Overview of auditory projection pathways and intrinsic microcircuits. In: The mammalian auditory pathways synaptic organization and microcircuits (Oliver DL, Cant NB, Fay RR, Popper AN, eds), pp 7-39. New York: Springer.

Oliver DL, Winer JA, Beckius GE, Saint Marie RL (1994) Morphology of gabaergic neurons in the inferior colliculus of the cat. J Comp Neurol 340:27-42.

Olthof-Bakker BMJ, Lyzwa D, Gartside SE, Rees A (2017) Evidence that the tinnitus-inducing agent salicylate has a direct effect on neural activity in the inferior colliculus. In, p 509. Assoc. Res. Otolaryngol. Abs.:.

Orton LD, Rees A (2014) Intercollicular commissural connections refine the representation of sound frequency and level in the auditory midbrain. eLife 2014;3:e03764.

Palmer AR, Shackleton TM, Sumner CJ, Zobay O, Rees A (2013) Classification of frequency response areas in the inferior colliculus reveals continua not discrete classes. J Physiol 591:4003-4025.

Patel CR, Zhang H (2014) Local application of sodium salicylate enhances auditory responses in the rat's dorsal cortex of the inferior colliculus. Front Neurol 5:235.

Rees A (1990) A closed-field sound-system for auditory neurophysiology. Journal of Physiology-London 430: P6.

Russwurm M, Wittau N, Koesling D (2001) Guanylyl cyclase/PSD-95 interaction: Targeting of the nitric oxide-sensitive alpha2beta1 guanylyl cyclase to synaptic membranes. J Biol Chem 276:44647-44652.

Serulle Y, Zhang S, Ninan I, Puzzo D, McCarthy M, Khatri L, Arancio O, Ziff EB (2007) A GluR1-cgkii interaction regulates AMPA receptor trafficking. Neuron 56:670-688.

Sheng M, Hoogenraad CC (2007) The postsynaptic architecture of excitatory synapses: A more quantitative view. Annu Rev Biochem 76:823-847.

Shibuki K, Okada D (1991) Endogenous nitric oxide release required for long-term synaptic depression in the cerebellum. Nature 349:326.

Slee SJ, David SV (2015) Rapid task-related plasticity of spectrotemporal receptive fields in the auditory midbrain. J Neurosci 35:13090-13102.

Song RS, Tolentino R, Sobie EA, Neves-Zaph SR (2016) Cross-regulation of phosphodiesterase 1 and phosphodiesterase 2 activities controls dopamine-mediated striatal α-amino-3-hydroxy-5-methyl-4-isoxazolepropionic acid (AMPA) receptor trafficking. J Biol Chem 291:23257-23267.

Steinert JR, Robinson SW, Tong H, Haustein Martin D, Kopp-Scheinpflug C, Forsythe Ian D (2011) Nitric oxide is an activity-dependent regulator of target neuron intrinsic excitability. Neuron 71:291-305.

632 Steinert JR, Kopp-Scheinpflug C, Baker C, Challiss RAJ, Mistry R, Haustein MD, Griffin SJ, Tong HX,
633 Graham BP, Forsythe ID (2008) Nitric oxide is a volume transmitter regulating postsynaptic
634 excitability at a glutamatergic synapse. Neuron 60:642-656.
635 Suga N, Ma XF (2003) Multiparametric corticofugal modulation and plasticity in the auditory system.
636 Nat Revs Neurosci 4:783-794.
637 Szabadits E, Cserép C, Ludányi A, Katona I, Gracia-Llanes J, Freund TF, Nyíri G (2007) Hippocampal
638 gabaergic synapses possess the molecular machinery for retrograde nitric oxide signaling. J
639 Neurosci 27:8101-8111.
640 Valtschanoff JG, Weinberg RJ (2001) Laminar organization of the NMDA receptor complex within the
641 postsynaptic density. J Neurosci 21:1211-1217.
642 Watson RE, Wiegand SJ, Clough RW, Hoffman GE (1986) Use of cryoprotectant to maintain long-term
643 peptide immunoreactivity and tissue morphology. Peptides 7:155-159.
644 Yan W, Suga N (1998) Corticofugal modulation of the midbrain frequency map in the bat auditory
645 system. Nat Neurosci 1:54-58.
646 Yassin L, Radtke-Schuller S, Asraf H, Grothe B, Hershfinkel M, Forsythe ID, Kopp-Scheinpflug C (2014)
647 Nitric oxide signaling modulates synaptic inhibition in the superior paraolivary nucleus (spn)
648 via cGMP-dependent suppression of kcc2. Front Neural Circuits 8:65.
649 Young ED, Robert JM, Shofner WP (1988) Regularity and latency of units in ventral cochlear nucleus -
650 implications for unit classification and generation of response properties. J Neurophysiol
651 60:1-29.
652 Zhang HM, Kelly JB (2001) AMPA and NMDA receptors regulate responses of neurons in the rat's
653 inferior colliculus. J Neurophysiol 86:871-880.
654 Zheng Y, Seung Lee H, Smith PF, Darlington CL (2006) Neuronal nitric oxide synthase expression in
655 the cochlear nucleus in a salicylate model of tinnitus. Brain Res 1123:201-206.